



HAL
open science

Revisited analysis of the PUIREX 2008 decay heat experiment in the Phénix Sodium Fast Reactor

Dorian da Cunha, Frédéric Nguyen, Jean-François Lebrat, Christophe Le Niliot

► **To cite this version:**

Dorian da Cunha, Frédéric Nguyen, Jean-François Lebrat, Christophe Le Niliot. Revisited analysis of the PUIREX 2008 decay heat experiment in the Phénix Sodium Fast Reactor. *Annals of Nuclear Energy*, 2024, 205, pp.110537. 10.1016/j.anucene.2024.110537 . hal-04581573

HAL Id: hal-04581573

<https://hal.science/hal-04581573>

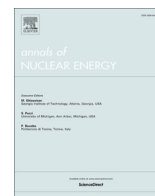
Submitted on 21 May 2024

HAL is a multi-disciplinary open access archive for the deposit and dissemination of scientific research documents, whether they are published or not. The documents may come from teaching and research institutions in France or abroad, or from public or private research centers.

L'archive ouverte pluridisciplinaire **HAL**, est destinée au dépôt et à la diffusion de documents scientifiques de niveau recherche, publiés ou non, émanant des établissements d'enseignement et de recherche français ou étrangers, des laboratoires publics ou privés.



Distributed under a Creative Commons Attribution - NonCommercial - NoDerivatives 4.0 International License



Revisited analysis of the PUIREX 2008 decay heat experiment in the Phénix Sodium Fast Reactor

Dorian da Cunha^{a,*}, Frédéric Nguyen^a, Jean-François Lebrat^a, Christophe Le Niliot^b

^a IRESNE, CEA, Cadarache, Saint-Paul-lez-Durance 13108, France

^b Aix Marseille Univ., CNRS, IUSTI, Technopôle de Chateau-Gombert, 5, rue Enrico Fermi, Marseille Cedex 13 13453, France

ARTICLE INFO

Keywords:

Decay heat
Sodium Fast Reactor
Phénix
Experiment
Validation
Uncertainty

ABSTRACT

Fast neutron reactors are of particular interest in the context of reducing carbon emissions, as they offer an attractive uranium economy and are crucial for closing the fuel cycle. To construct new reactors, safety issues must be studied thoroughly, and decay heat is a critical parameter, as demonstrated during the Fukushima accident. To ensure reactor safety, it is necessary to know the decay heat throughout the fuel cycle. Calculation tools are being developed at CEA and have been validated by comparing them with experiments performed in Sodium Fast Reactors Phénix and Superphénix. For many years, there have been inconsistencies between the experimental and calculated decay heat values for French SFRs. The analysis of the 2008 PUIREX experiment in Phénix has been revisited, and a new method has been tested to obtain the decay heat from temperature measurements. Explanations for the discrepancies with the calculations have been found.

1. Introduction

Decay heat is a crucial parameter for nuclear reactor and fuel sub-assembly safety. It is the energy released by the decay of unstable nuclides present in the fuel or produced by its irradiation, spontaneous fissions, and delayed neutrons. It accounts for up to 7% of the reactor's power just before shutdown. The French Nuclear Safety Authority identifies the removal of decay heat as one of the three fundamental safety functions. If this function is not insured, the core may melt, resulting in a severe accident. The increasing interest in nuclear reactors for their low-carbon energy production implies a growing focus on fast neutron reactors. They have an attractive uranium economy and are essential for closing the fuel cycle.

Decay heat experiments have been carried out for decades for both thermal fissions (Shure, 1961; Schrock, 1979) and fast fissions (Akiyama, 1982; Aoyama, 1999; Lott, 1972; Fisher et al., 1964). Neutronics and depletion codes are used to compute decay heat results, which are compared to measurements for validation (England, 1962; Bell, 1973; Tasaka, 1977; Kolobashkin et al., 1983; Duchemin et al., 1990; Grouiller et al., 1990; Gomin, et al., 1999; Tsilanizara et al., 2000). Two main methods have been developed to experimentally evaluate decay heat. The calorimetric method involves using the first law of thermodynamics to deduce the decay heat of an irradiated

material (Johnston, 1964). While the method is straightforward, measuring short cooling time can be challenging due to the thermal response of the calorimeter. Many experiments (Lott et al., 1972; Schrock, 1979; SKB, 2006) have employed this method by measuring temperature increases, heat flows and temperature differences. Another method involves using spectrometers to measure the energy of β and γ rays emitted by the irradiated material (Dickens, 1977; Nguyen, 1997). To obtain an accurate measurement of the decay heat and avoid the Pandemonium effect (Hardy et al., 1977), this method requires highly efficient detectors sensitive to both γ and β rays (Maekawa et al., 2000; Algora, et al., 2010; Guadilla et al., 2016).

For a considerable period, the majority of irradiated materials were samples weighing between a few milligrams and a few grams, consisting of element of interest such as ^{235}U , ^{238}U or ^{239}Pu and with a purity level of approximately 90 % (Dickens, 1977; Dickens, et al., 1981; Fisher et al., 1964). These samples underwent short-term irradiation and were promptly retrieved for measurement. To calculate accurately the energy released per fission, it is necessary to characterise the neutron flux and neutron spectrum at the irradiation position. These small and pure samples cannot fully relate the physics of a complete fuel element. However, measuring the decay heat of a whole fuel element is a complex logistical task, and there are few experiments that have been conducted on this topic, (Ilas, 2008; Svensk Kärnbränslehantering, 2006; Jaboulay et al., 2012), particularly in relation to fast reactor fuel (Maekawa et al.,

* Corresponding author.

E-mail address: dorian.dacunha@cea.fr (D. da Cunha).

Nomenclature			
Acronyms			
C/E	Calculation to Experiment	t	Time (s)
MOX	Mixed OXide fuel	Sources	Thermal sources (kW)
OLS	Ordinary Least Squares	θ	Sodium temperature (K); $\theta_0 = 400^\circ\text{C}$ and $\theta_1 = 357^\circ\text{C}$ are reference temperatures
PWR	Pressurized Water Reactor	ρ_i	Density of material i ($\text{kg}\cdot\text{m}^{-3}$)
SFR	Sodium-cooled Fast Reactor	λ_i	Decay constant of isotope i (s^{-1})
Symbols		$\text{Var}(t)$	Variance of variable t (s^2)
C_1	Nominal rotation speed of primary pumps (r.p.m)	V_i	Rotation speed of pump i (r.p.m)
C_2	Nominal rotation speed of secondary pumps (r.p.m)	η_{pp}, η_{sp}	Primary and secondary pumps' yields at nominal power
$\text{Cov}(\theta, t)$	Covariance between variables θ and t (K.s)	Devices	
$c_{pi}(\theta)$	Specific heat capacity of material i ($\text{kJ}\cdot\text{kg}^{-1}\cdot\text{K}^{-1}$)	cc	Cold collector
E_i	Mean decay energy of isotope i (J)	heater	Under vessel heaters
I	Thermal inertia ($\text{kJ}\cdot\text{K}^{-1}$)	Pheater	Primary regular circuit heater
Leaks	Thermal leaks (kW)	PPC	Primary purification circuit
L_i	Thermal leak from device i (kW)	Rheater	Last resort circuit heater
m_i	Mass of material i (kg)	SPC	Secondary purification circuit
N_i	Amount of isotope i	trap	Steam generator trap doors
$P(t)$	Decay heat at time t (kW)	hc	Hot collector
P_{device}	Power coming from a specified device (kW)	LastResort	Last resort circuit
P_{pi}	Electrical power powering primary pump i (kW)	pp	Primary pumps
P_{si}	Electrical power powering secondary pump i (kW)	primary	Primary circuit
r^2	Coefficient of determination	sp	Secondary pumps
		Spipe	Secondary circuit piping
		slab	Primary slab

Table 1
Review of the decay heat measurements in French SFRs.

Decay heat experiments and their comparisons to calculations			
Reactor and year of the experiment	Cooling time	Year of the calculation	Discrepancy between the experiment and the latest calculation
Phénix 1979 (Desperts, 1979)	7 to 36 h	1979 and 1992 ¹ (Gillet, 1992)	+6 to +20 %
Phénix 1982 (Guidez, 1983)	6 to 28 h	1983	-12 to -8 %
Phénix 1993 (Martin, 1993)	6 to 72 h	1993 (Gillet, 1993)	+5 to +17 %
Phénix 2008 (Auban, 2008), (Chauchepreat et al., 2008)	1.5 h to 12 days	2012 (Benoit et al., 2012) and 2016 ¹ (Lebrat, et al., 2016)	-6 to +26 %
Superphénix 1987 (Gillet, 1987; Gillet et al., 1990)	3 to 24 h	1988 (Gillet, 1988), 1996 (Gillet, 1996) and 2020 ¹ (Calame et al., 2020)	-20 to -8 %
Superphénix 1996	3 to 84 h	1998 (Bernardin, 1998) and 2002 ¹ (Bourdote, 2002)	-10 to -5 %

¹ Several dates of calculation appear when an update of the calculation has been carried-out.

2000). This paper discusses an experiment that measures the decay heat of an entire nuclear core.

In the 70's and 80's, France built the Phénix and Superphénix Sodium Fast neutron Reactors (SFR) and numerous decay heat experiments were carried out to demonstrate the feasibility, viability and safety of such reactors. The measurements, as summed up in Table 1 took place in 1979, 1982, 1993 and 2008 in Phénix and in 1987 and 1996 in Superphénix. Each measurement has been compared with computations and the discrepancies are different in each case – showing no clear tendency – and relatively high. The 2008 experiment shows a bias in the Calculation to Experiment ratio (Benoit et al., 2012) and an important

discrepancy at early time, as shown in Fig. 1. For this reason, a new calculation was performed in 2018 (Lebrat et al., 2018) with the up to date depletion package DARWIN-2 (Tsilanizara et al., 2000) and the associated nuclear data library JEFF 3.1.1 (NEA, 2009), but no improvement of the C/E was observed. This work aims to understand the persisting discrepancy between the 2008 decay heat measurement in Phénix and the calculations. We present an overview of the experimental decay heat estimate method, followed by a short description of the Phénix reactor. Then, the previous experimental data analysis – on which we relied during the study – will be presented as well as the improvements we propose in order to estimate the experimental decay heat. Finally, we present new results, as we identified some sources of bias in the experimental data processing.

2. The experimental data and their analysis

2.1. Estimate of the experimental decay heat

Direct measurement of decay heat from a nuclear core is not yet possible. Therefore, the thermal balance equation (1) is crucial for indirectly estimating decay heat in a nuclear reactor experiment, where temperature is measured over time.

$$I(\theta) \frac{\partial \theta}{\partial t} = P_{decay\ heat}(t) + Sources(\theta) - Leaks(\theta) \quad (\text{kW}) \quad (1)$$

The determination of experimental decay heat requires knowledge of the temperature variation rate and all thermal contributions, including sources and leaks. These contributions are temperature-dependent due to the thermal dependence of material properties and pump efficiency. To obtain the decay heat from the measured temperatures, a thermal balance of the entire reactor is achieved in this experiment. The simplified 'point' model represents the entire reactor, with a single temperature considered in the thermal balance to estimate thermal sources, leaks, and the rate of temperature variation.

Developing a reliable thermal model necessitates additional experiments, which are challenging to design and must be executed with care, using appropriate instrumentation. Consequently, there are few thermal

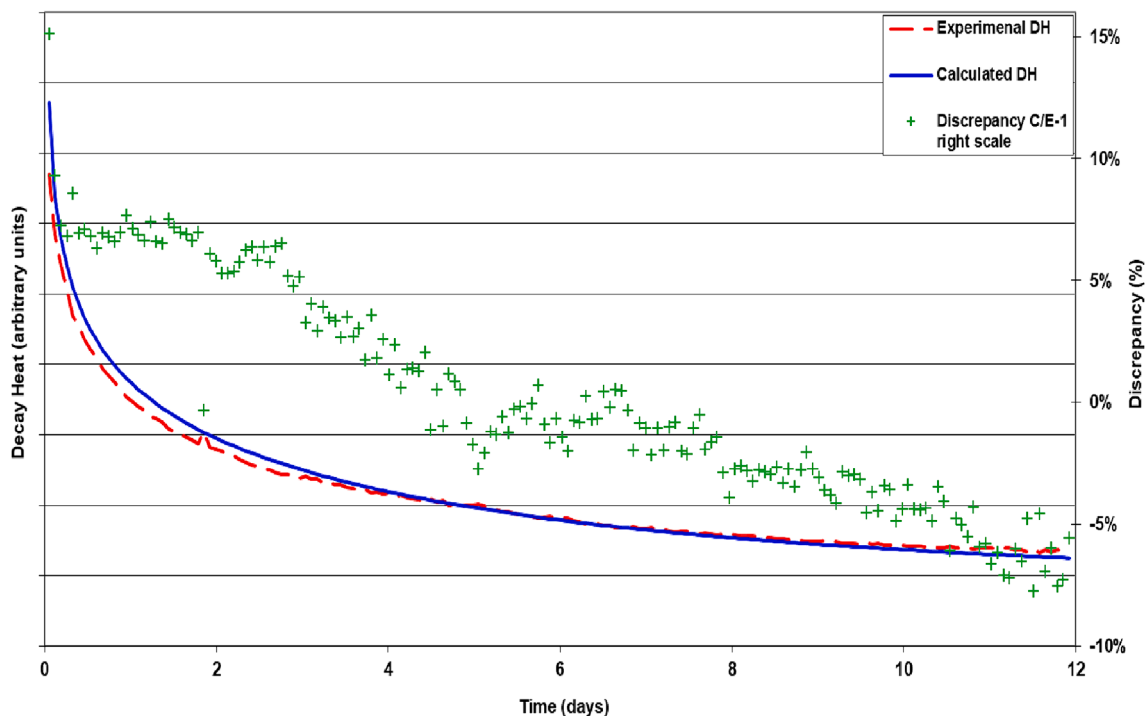


Fig. 1. Results of the 2012 estimate of the experimental decay heat (continuous blue curve) compared to the 2012 calculation (dotted red curve) with the C/E-1 reported on the right axis (green crosses) (Benoit et al., 2012). (For interpretation of the references to colour in this figure legend, the reader is referred to the web version of this article.)

models available, which frequently restricts the range of physical models that can be used to calculate thermal balance. Decay heat experiments typically involve cooling the subassembly or core with a heat-transfer fluid. In our case, an accurate estimation of the reactor's thermal inertia as a function of its temperature requires precise knowledge of the reactor.

Table 1 presents the decay heat experiments. These experiments were used to develop feedback for estimating thermal inertia, thermal modelling for leaks or sources, and determining relevant positions for temperature measurements in the 2008 Puirex experiment.

As previously mentioned, accurately estimating the experimental decay heat of an entire nuclear reactor core requires several steps. This is a complex task as the reactor core is not a calorimeter, but rather a sophisticated environment that is difficult to model accurately. The following section outlines the key components of Phénix that are crucial for accurate decay heat estimate.

2.2. Description of the Phénix reactor

Phénix is a 350 MWt (megawatts thermal) Sodium-cooled Fast Neutron Reactor (SFR) that began operation in 1973 and shut down in 2010. The reactor is integrated, with a single vessel containing all primary circuit components (Guidez, 2013).

2.2.1. Primary circuit

Two vessels compose the primary circuit, as illustrated in Fig. 2. The main vessel contains the primary circuit, including six sodium-sodium heat exchangers, three mechanical pumps, the “cold” sodium and the primary vessel. The volume containing cold sodium is called “cold collector”. The primary vessel contains the core, the “hot” sodium and the rotating cap, which is instrumented. The volume containing hot sodium is denoted “hot collector”. A thermally insulated vessel contains the whole and a vessel having its own cooling system in case of accident, the last resort circuit, contains the thermally insulated vessel.

2.2.2. Secondary circuits

There are three secondary circuits, S1, S2 and S3, each consisting of: its own pump, two sodium-sodium heat exchangers located in the main vessel and a steam generator. Fig. 3 shows a schematic diagram of one of these secondary circuits. After the decrease of power from 560 MWt to 350 MWt, imposed by the safety regulations, the S2 secondary circuit was shut down and its heat exchangers were replaced by fake ones shown in Appendix 1. Only secondary circuits S1 and S3 remained in use.

2.2.3. Auxiliary circuits

There are auxiliary circuits for both the primary and secondary circuits. There is a sodium purification circuit dedicated to the primary circuit: it cools the sodium with cold traps to precipitate impurities, filters them and then heats the sodium before returning it to the primary circuit. As for the secondary circuits, there is a sodium purification circuit and a hydrogen detection circuit for each of them. Both types of circuits include thermal leakages and heating systems.

2.3. Sequence of events of the PUIREX 2008 experiment

On May 15th 2008, the primary and secondary cold traps of the purification sodium circuit were bypassed in order to minimise thermal leakages.

On May 16th at 3 p.m., a scram stopped the chain reaction with a 45-second control rod drop, after an irradiation equivalent to 71,08 effective full power days (efpd). A 12-day decay heat experiment began. Operators cooled the sodium to a temperature of 370 °C, to bring the reactor to safe conditions. They, then dried the two steam generators and prevented heat exchange with the outside. The reactor was then considered as a calorimeter, with little heat transfer to the outside. The temperature was homogenised thanks to the primary and secondary pumps still in operation. One day later, the operators reduced the speed of the secondary pumps and the day after, the speed of the primary pumps. Five days after the rapid stop, they emptied the S3 secondary

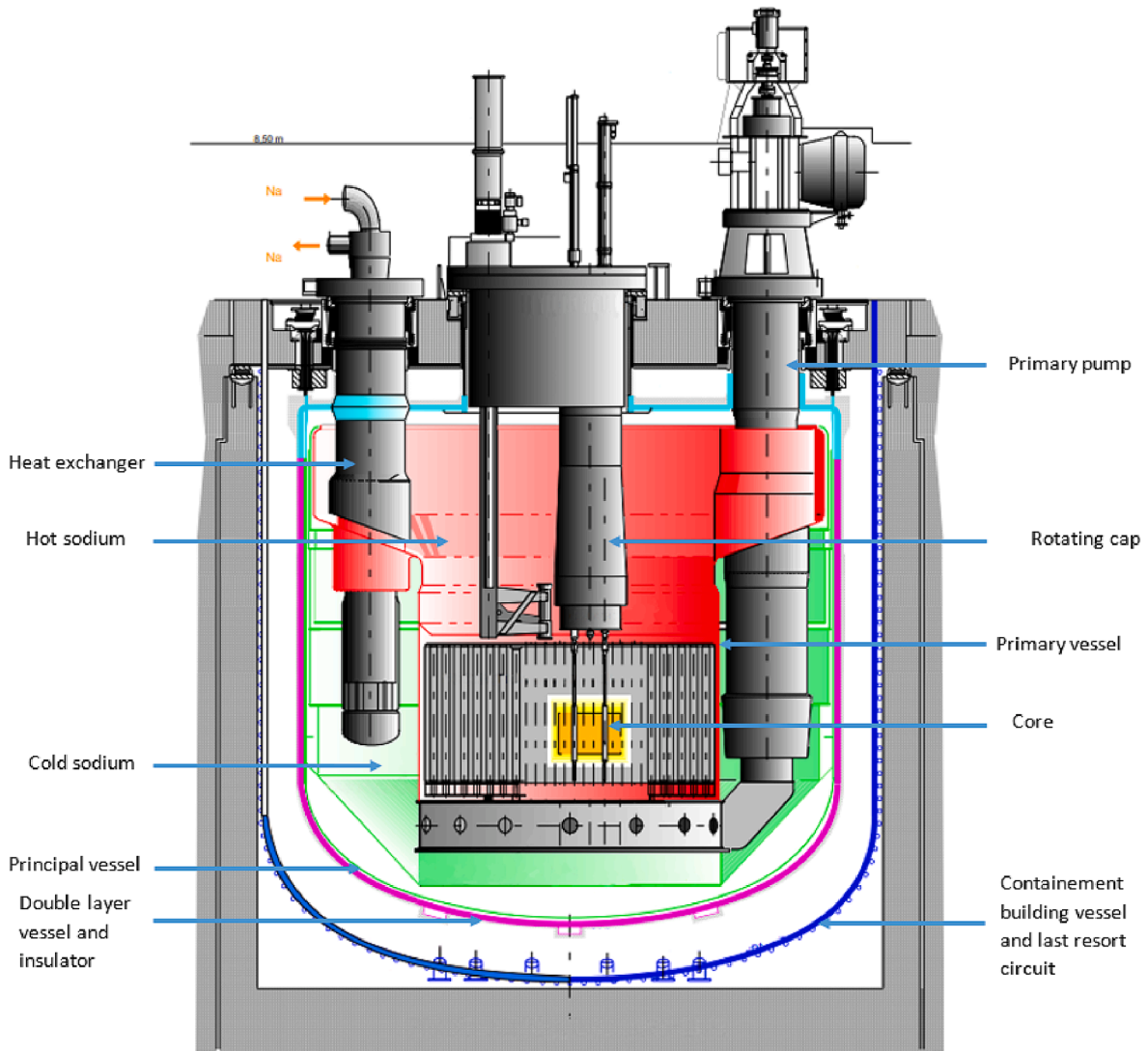


Fig. 2. Axial section view of the Phénix primary sodium circuit.

circuit and after 12 days of experiment, the steam generators trapdoors were opened to cool the sodium: this was the end of the experiment. The exact sequence of events is as follows:

- t_0 : May 16th 2008, 3p.m, fall of the control rods
- $t_0 + 33 \text{ min}$: Primary sodium purification circuit put in low regime mode, in order to minimize its thermal leaks
- $t_0 < t < t_0 + 62 \text{ min}$: Cooling of the sodium to $370 \text{ }^\circ\text{C}$; primary pumps operating at 540 r.p.m
- $t_0 + 62 \text{ min}$: Both steam generators are dried, the secondary circuits are not cooled anymore
- $t_0 + 70 \text{ min} < t < t_0 + 2779 \text{ min}$: Primary pumps operate at 300 r.p.m
- $t_0 + 2796 \text{ min} < t < t_{end}$: Primary pumps operate at 110 r.p.m
- $t_0 + 1026 \text{ min} < t < t_{end}$: Secondary pumps operate at 100 r.p.m instead of 110 before. The pump of the S3 circuit is stopped after 5 days, when the operators empty the S3 circuit.

It is highly important to underline the lack of a criterion to define a precise “start of experiment”, when the reactor can be considered as isothermal. Thus, during the post-processing of the decay heat estimate, the experimenters chose the virtual “start” of the experiment at some point. This lack of traceability of the subjective criterion led in this case to a “time shift” resulting in important discrepancies between

experimental and computational results, as we will discuss in paragraph 4.

2.4. Data acquisition

During the experiment, the temperatures were measured throughout the reactor with dozens of thermocouples. Of all the thermocouples, 59 were placed on two instrumented poles, one in the hot collector: ML03; the other in the cold collector: EIM. Appendix 1 is a horizontal section of the primary circuit and shows the position of the poles, which measure temperature at a frequency of 0.1 Hz. Of the 59 thermocouples available, the experimenters selected 13 of them to represent an average temperature of the sodium in the hot collector. The evolution of this average temperature during the experiment is displayed in Fig. 4. After the drying of the steam generators, the temperature increased, as decay heat was considerable. It then reached a maximum of $396 \text{ }^\circ\text{C}$ and began to fall: the decay heat decreased exponentially and no longer compensated for thermal leakages. Slope discontinuities allow us to detect the changes in the operating mode of the reactor that we mentioned in paragraph 2c.

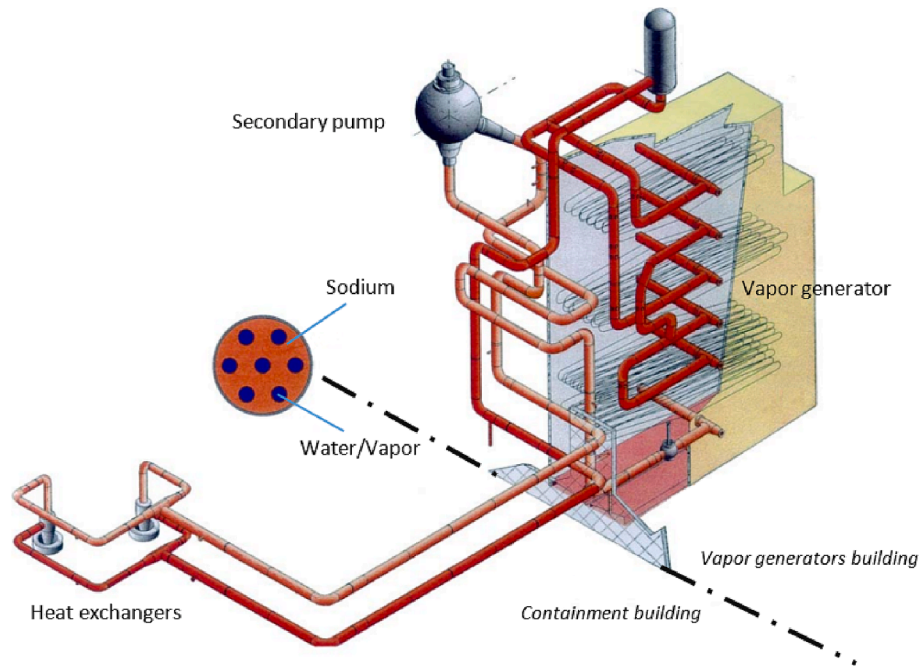


Fig. 3. Representation of a Phénix secondary sodium circuit.

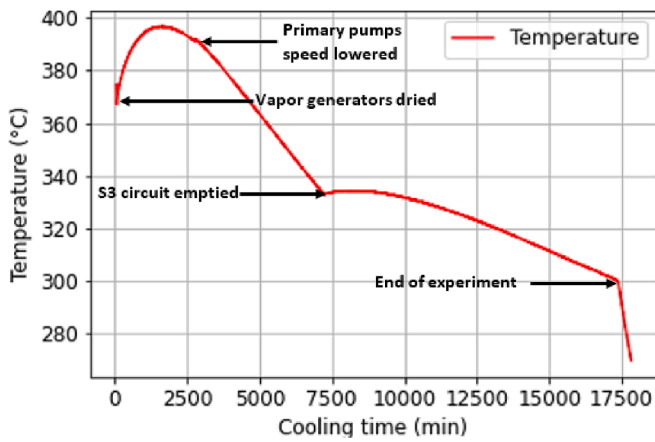


Fig. 4. Mean temperature in the primary circuit obtained during the PUIREX experiment in the Phénix reactor. 13 thermocouples were used to represent a mean temperature of the sodium.

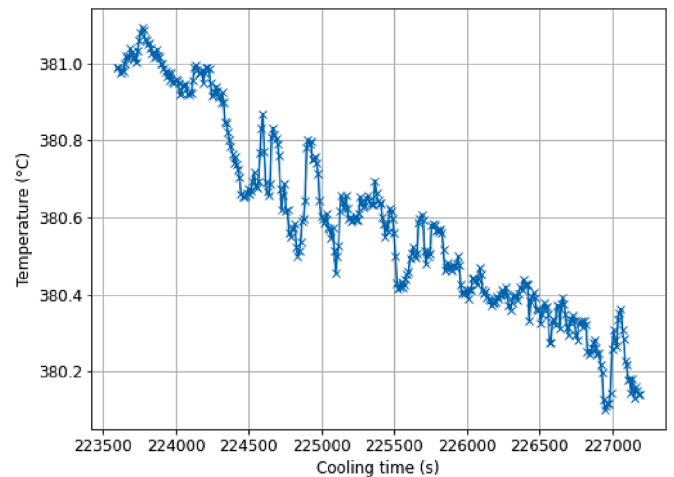


Fig. 5. Mean temperature of the Phénix primary circuit sodium during the PUIREX experiment.

3. Indirect determination of the experimental decay heat

3.1. Processing of data

Fig. 5 shows an example of the mean temperature evolution as a function of time. Temperatures in Fig. 5 match the initial temperatures displayed in Fig. 6 where temperature fluctuations are difficult to assess due to the larger time scale. Since we did not know whether the observed fluctuations were due to a physical phenomenon – such as an inhomogeneous sodium temperature – or to some noise in the data acquisition, we decided to extract the temperatures from 223 600 s to 303 600 s and study them in more detail. We chose this interval because the temperature appears to follow a straight line and is easier to model. We then calculated a linear model to fit these data and we found a good agreement, as shown in Fig. 6.

The coefficient of determination r^2 shows that there is a good agreement between the linear regression and the data, so we calculated the difference between both (see residuals Fig. 7) in order to understand

the behaviour of the temperature over a short time scale. We sorted the discrepancies we obtained and divided them into ten intervals with the same number of values in each interval. This gave us nine quantiles Q_i separating intervals with equal probabilities.

We compared these values with those of the standard normal distribution. Fig. 8 represents on the y-axis the quantiles of the standard normal distribution related to the cumulative frequency of the experimental quantiles obtained. On the x-axis, there are the quantiles of the temperature discrepancies we obtained. We use this Quantile-Quantile (Q-Q) plot as a graphical test for data analysis (Jockey, 1963; Wilk et al., 1968). Since it follows a straight line as shown by the value of the coefficient of prediction r^2 , there is clearly a good match between both distributions, which means that the observation is most likely a Gaussian noise with a mean close to 0 and a standard deviation of around $0.03^\circ\text{C}/h$, probably due to the electronics used for the measurement and signal amplification.

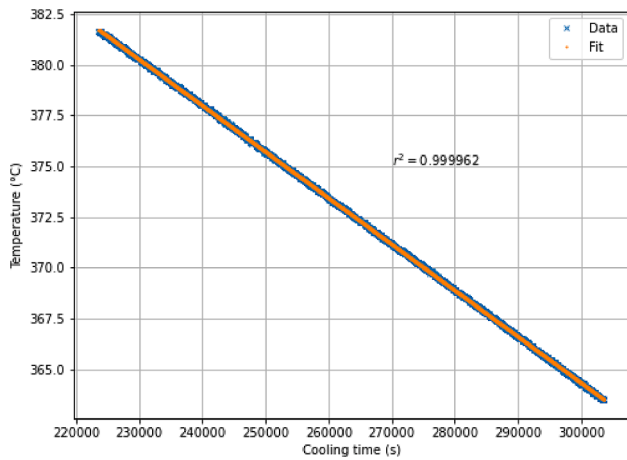


Fig. 6. Mean temperature measured in the Phénix primary circuit sodium during the PUIREX experiment and the associated linear fit with its coefficient of determination r^2 .

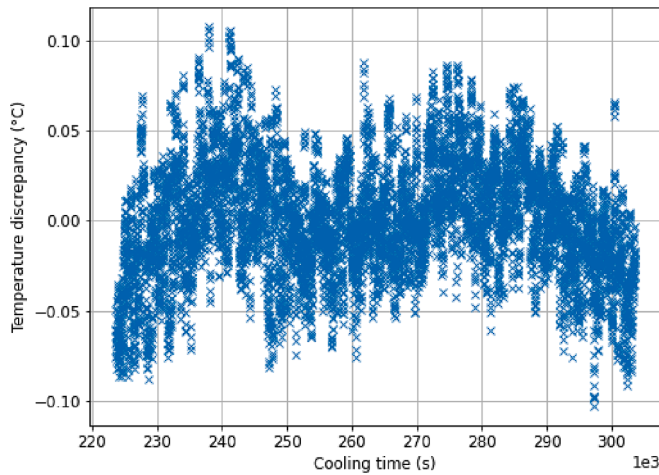


Fig. 7. Discrepancy between the temperature raw measurement and the linear fit.

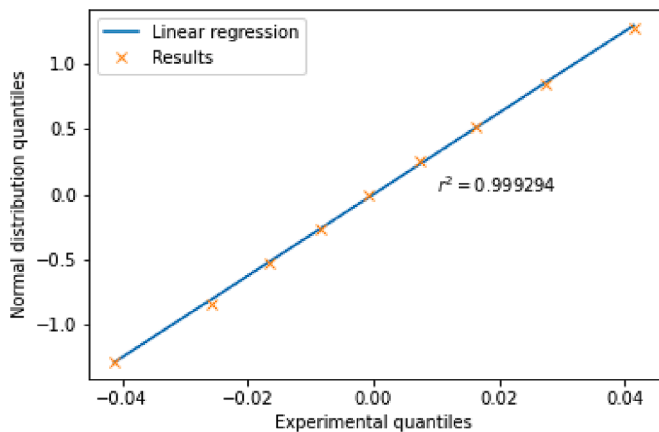


Fig. 8. Normal probability plot of residuals with a coefficient of determination r^2 regarding the linear fit of the distribution close to 1.

Table 2

Masses of the different materials in the Phénix reactor.

Material	Sodium	Steel	Graphite	Fuel
Mass (ton)	1000	1050	74	17

3.2. Thermal model used to estimate the decay heat

In the interpretation of this experiment, a point model represents the reactor temperature as mentioned in paragraph 2.a. Experimenters decided to select 13 thermocouples from the two poles in the reactor, to have a good representation of a mean temperature in the primary circuit. They then considered the whole reactor to be isothermal, which means that the temperature used for the decay heat estimate is a mean temperature that is supposed to represent the whole reactor. In this way, a unique temperature is used in each thermal model and equation (1) can be applied. The thermal balance is calculated thanks to the thermal inertia, thermal leakages and thermal sources (of which the decay heat is one). Since decay heat is the unknown parameter we want to determine, we obtain equation (2).

$$DecayHeat(t) = I(\theta) \frac{\partial \theta}{\partial t} - Sources(\theta) + Leaks(\theta) (kW) \quad (2)$$

The thermal inertia of the reactor is calculated as follows:

$$I(\theta) = \sum_i m_i c_{pi}(\theta) (kJ.K^{-1}) \quad (3)$$

The different specific heat capacities are obtained using equations (4)¹:

$$C_{pNa}(\theta) = 1.436715 - 5.805379 \cdot 10^{-4} \theta + 4.627274 \cdot 10^{-7} \theta^2 \quad (\text{Foust, 1972}) \quad (4a)$$

$$C_{psteel}(\theta) = 0.4676 + 3 \cdot 10^{-4} \theta - 2 \cdot 10^{-7} \theta^2 \quad (kJ.kg^{-1}.K^{-1}) \quad (4b)$$

$$C_{pgraphite} = 1.300 \quad kJ.kg^{-1}.K^{-1} \quad (4c)$$

$$C_{pff}^1 = 0.234 \quad kJ.kg^{-1}.K^{-1} \quad (4d)$$

Masses of the different reactor components are summed-up in Table 2.

3.3. Available models of the thermal balance

3.3.1. The “ETNa” thermal model

In the past, Phénix operators used the ETNa code (Dumarcher et al., 2008) to estimate the time required for the sodium to reach a specific temperature that would allow handling of the subassemblies. Based on a simplified decay heat model and a mean reactor temperature, the code provides the evolution of the mean temperature in the reactor thanks to successive thermal balance calculations. ETNa – which had been validated on previous experiments (Appere, 1998) – was used in (Benoit et al., 2012) to estimate the decay heat during the PUIREX experiment. Equations (5) to (16) are those used in ETNa, where equation (5) being equation (1) developed with a different thermal model.

$$\frac{\partial \theta}{\partial t} = \frac{P_{decayheat}(t) + P_{pp} + P_{sp} + P_{heater} - L_{slab} - L_{lastResort}}{I(\theta)} + \frac{-L_{ppc} - L_{spipe} - L_{spc} - L_{rap}}{I(\theta)} \quad (5)$$

$$P_{pp} = \sum_{i=1}^3 \frac{P_{pi}}{3} \left(\frac{\rho_{Na}(\theta)}{\rho_{Na}(\theta_0)} \right) \left(\frac{V_i}{C_1} \right)^3 + \frac{P_{pi}}{3} \left(\frac{1}{\eta_{pp}} - 1 \right) \left(\frac{\rho_{Na}(\theta)}{\rho_{Na}(\theta_0)} \right)^2 \left(\frac{V_i}{C_1} \right)^4 (kW) \quad (6)$$

¹ fissile fuel specific heat capacity.

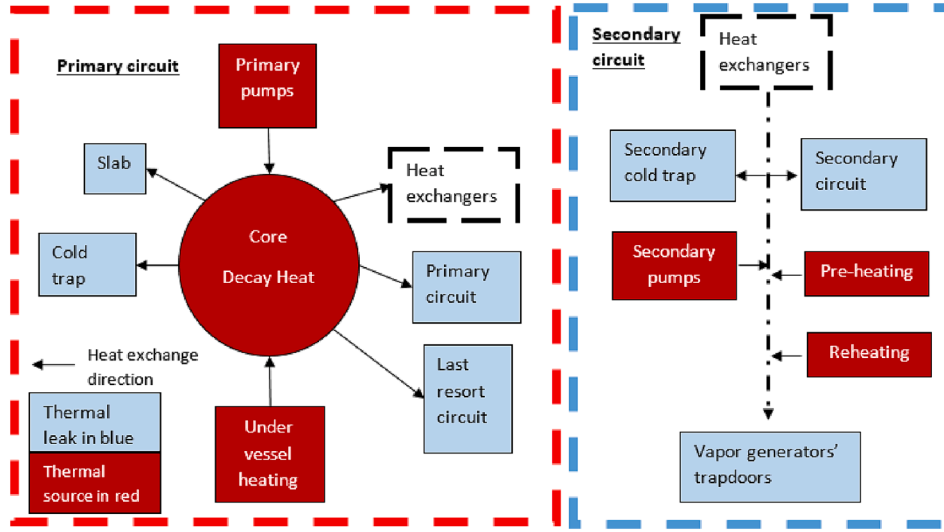


Fig. 9. Schematic representation of the thermal balance in the Phénix reactor for the primary circuit and one secondary circuit. (Thermal leaks are colored in blue and thermal sources in red). (For interpretation of the references to colour in this figure legend, the reader is referred to the web version of this article.)

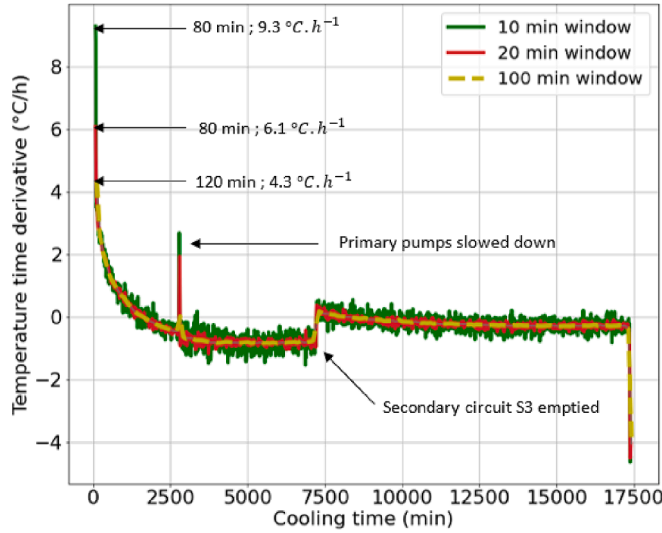


Fig. 10. Impact of the regression window size on the time derivative of the temperature.

$$P_{sp} = \sum_{i=1}^2 \frac{P_{si}}{3} \left(\frac{\rho(\theta)}{\rho_{Na}(\theta_1)} \right) \left(\frac{V_i}{C_2} \right)^3 + \frac{P_{si}}{3} \left(\frac{1}{\eta_{sp}} - 1 \right) \left(\frac{\rho_{Na}(\theta)}{\rho_{Na}(\theta_1)} \right)^2 \left(\frac{V_i}{C_2} \right)^4 \quad (kW) \quad (7)$$

where $C_1 = 720.5 \text{ r.p.m.}$, $C_2 = 908 \text{ r.p.m.}$, $\eta_{pp} = 0.864$ and $\eta_{sp} = 0.74$

$$\rho_{Na}(\theta) = 950.0483 - 0.2297537 \cdot \theta - 1.46045 \cdot 10^{-5} \theta^2 + 5.6377 \cdot 10^{-9} \theta^3 \quad (\text{Foust, 1972}) \quad (8)$$

$$P_{heater} = (P_{Pheater} + P_{Rheater}) \times 0.765 \quad (kW) \quad (9)$$

$$L_{slab} = 0.4 \cdot \theta - 8 \quad (kW) \quad (10)$$

The equation is valid only if the exit temperature of the last resort circuit is set to 28 °C.

$$L_{LastResort} = -0.45489 + 5.0116 \cdot 10^{-3} \theta - 1.2388 \cdot 10^{-5} \theta^2 + 1.8723 \cdot 10^{-8} \theta^3 \quad (kW) \quad (11)$$

$$L_{PPC} = \frac{Q}{3600} \rho_{Na} \cdot c_{pNa} \cdot \Delta\theta \quad (kW) \quad (12)$$

$$L_{Spice}(\theta) = 2 \times (230.9988 - 0.82 \cdot \theta + 0.003542 \cdot \theta^2 + C_3) \quad (kW) \quad (13)$$

$C_3 = 156 \text{ kW}$ is an experimental coefficient.

$$L_{SPC} = \frac{Q}{3600} \rho_{Na} \cdot c_{pNa} \cdot \Delta\theta \quad (kW) \quad (14)$$

$$L_{trap} = (0.0092 \cdot \theta - 0.51333) \times 10^3 \quad (kW) \quad (15)$$

$$\bar{\theta} = (\theta_{hc} - \theta_{cc}) \times 0.374 + \theta_{cc} \quad (^\circ\text{C}) \quad (16)$$

$\bar{\theta}$ is the initial temperature taken for computations in case of the unavailability of usual means of decay heat removal.

A schematic of the thermal balance in ETNa is represented in Fig. 9. Heat leaks are coloured blue and thermal sources are coloured red. Arrows indicate the direction of heat flow. The primary circuit is shown on the left of the figure in a red dashed square, while the secondary circuit shown on the right as a blue dashed square. One secondary circuit is shown instead of two, but they share the same architecture. The primary and secondary circuits communicate via heat exchangers, which are represented in both circuits by a black dashed square.

3.3.2. Adaptation of the thermal code to the PUIREX experiment

In order to adapt the ETNa model to a decay heat estimate, several changes have been made. First, the time derivative of the temperature has to become the input, instead of the decay heat. Second, for the PUIREX experiment, the thermal leakages and sources were minimised, as mentioned earlier in paragraph 2.c. Thus, cold traps of purification circuits were in low regime mode, with the vessel heaters turned off and the steam generators trapdoors closed. In this configuration, equations (12) and (14) do not appear in the thermal balance and make the estimate easier and more accurate. Equation (13) is adapted to the experiment, together with equation (17). The f function appears in equation (17) and is defined in equation (18). This function allows the emptying

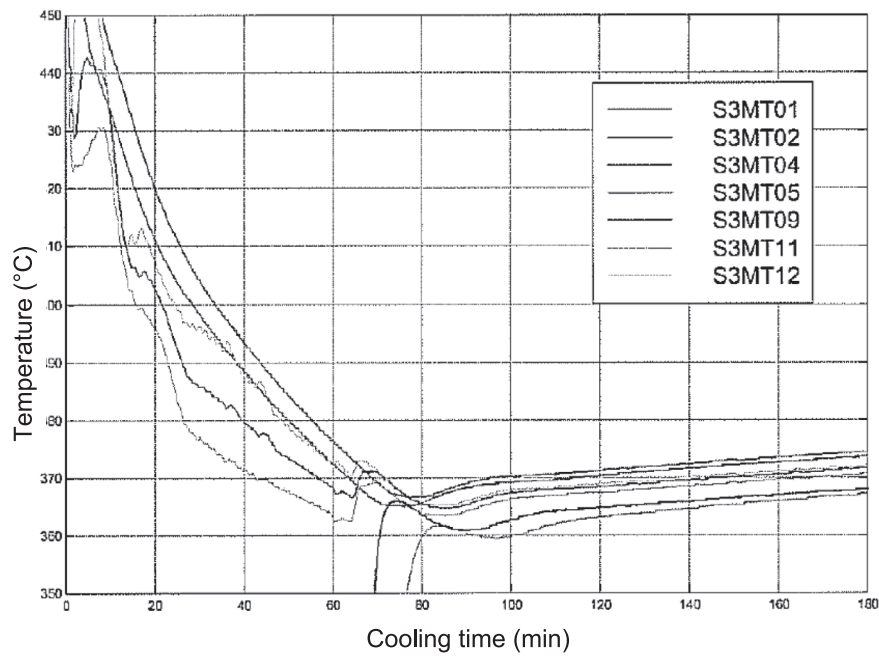


Fig. 11. S3 Secondary circuit temperature measurements during the first 3 h of the PUIREX experiment.

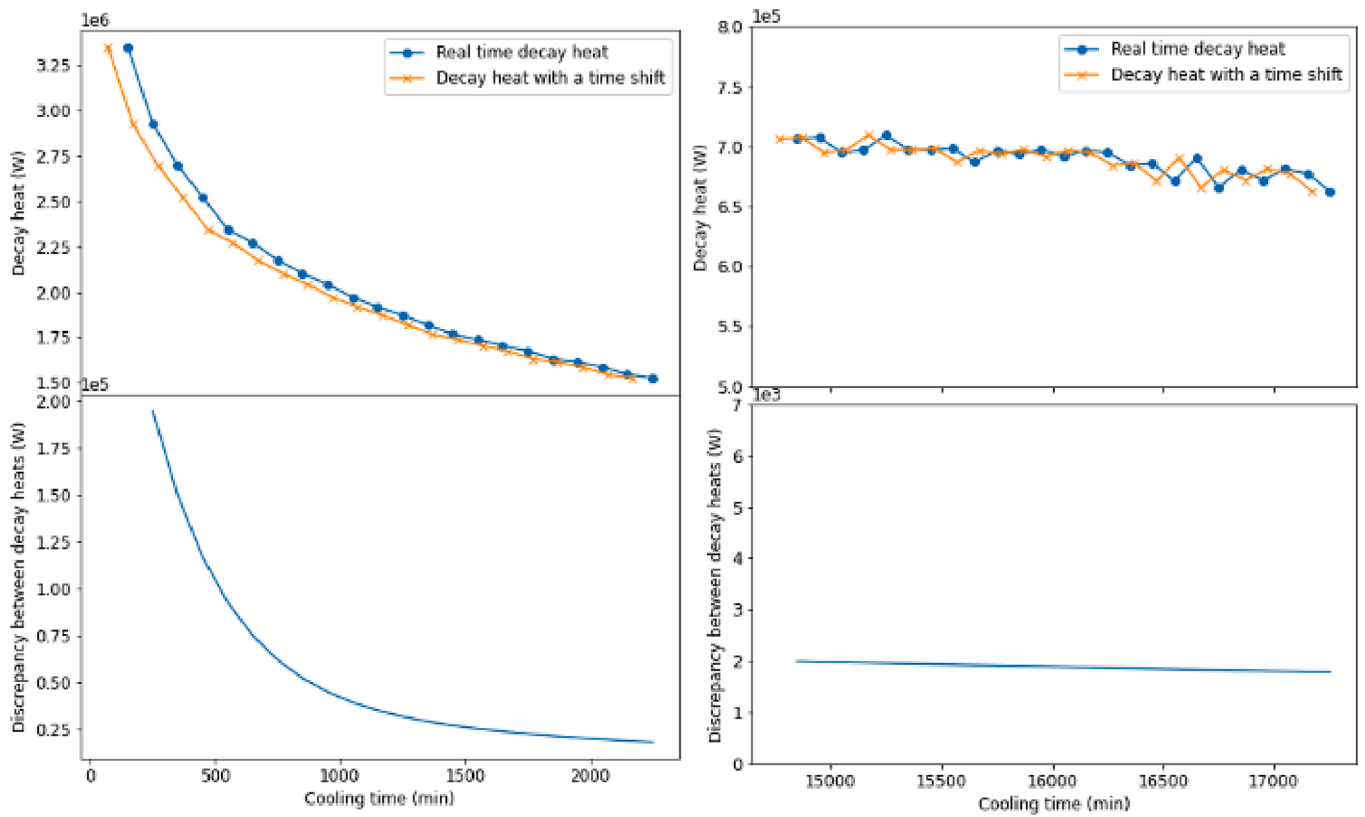


Fig. 12. Time shift effect on the decay heat and evolution of the induced bias.

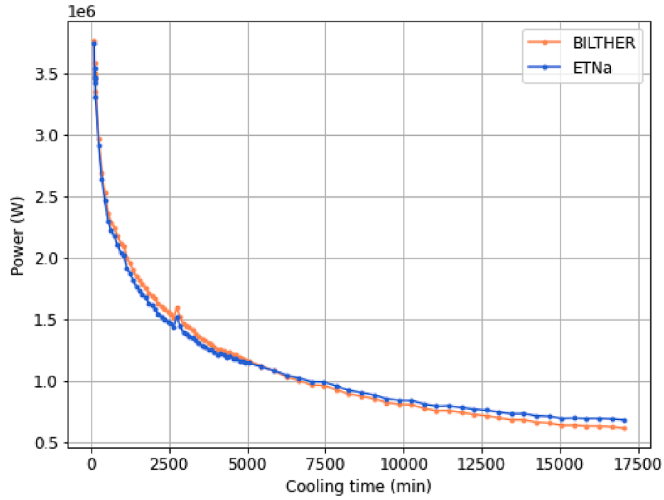


Fig. 13. Comparison of the PUIREX experimental decay heat estimates based on BILTHER and ETNa models.

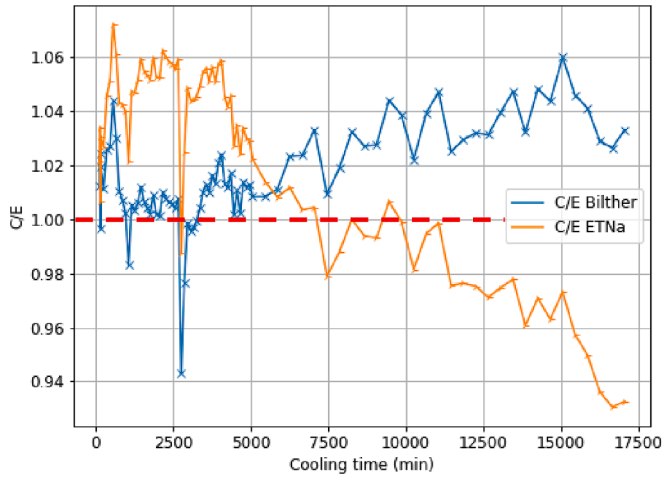


Fig. 14. C/E of the PUIREX decay heat with the BILTHER and the ETNa thermal models.

of the S3 secondary circuit to be modelled. Given this configuration, the results obtained are shown in Fig. 1 (Benoit, et al., 2012).

$$L_{secondary}(\theta) = (230.9988 - 0.82 \cdot \theta + 0.003542 \cdot \theta^2 + C_3) + f(t)(230.9988 - 0.82 \cdot \theta + 0.003542 \cdot \theta^2 + C_3) \quad (kW) \quad (17)$$

$$f(t) = H(t - t_0) - H(t - t_0 - 5 \text{ days}) \quad (18)$$

H being the Heaviside step function.

3.3.3. Suggested improvements to the thermal model

Firstly, we propose to implement a function f in the function equation (19) of the secondary pumps, in order to respect the modelling of the experiment, even if the corresponding contribution is very small.

$$P_{sp} = \frac{P_{s1}}{3} \frac{\rho(\theta)}{\rho_{Na}(\theta_1)} \left(\frac{V_i}{C_2}\right)^3 + \frac{P_{s1}}{3} \left(\frac{1}{\eta_{sp}} - 1\right) \left(\frac{\rho(\theta)}{\rho_{Na}(\theta_1)}\right)^2 \left(\frac{V_i}{C_2}\right)^4 + f(t) \left[\frac{P_{s2}}{3} \frac{\rho(\theta)}{\rho_{Na}(\theta_1)} \left(\frac{V_i}{C_2}\right)^3 + \frac{P_{s2}}{3} \left(\frac{1}{\eta_{sp}} - 1\right) \left(\frac{\rho(\theta)}{\rho_{Na}(\theta_1)}\right)^2 \left(\frac{V_i}{C_2}\right)^4 \right] \quad (kW) \quad (19)$$

Secondly, we found another modelling of the primary leaks given by another code used for the Phénix reactor called BILTHER (Coulon, 2010). This code was used to estimate the power of the plant thanks to the thermal balance in the tertiary circuit. In this code, the primary and secondary leaks are still temperature dependent, which has also been validated with previous experiments. In this code, the primary thermal leaks are given by equation (20).

$$L_{primary}(\theta) = L_{hc} + L_{cc} \quad (kW) \\ = -4.56 + 0.21 \cdot \theta + 1.25 \cdot 10^{-4} \theta^2 + 403.9 - 6.69 \cdot \theta + 1.025 \cdot 10^{-2} \theta^2 \quad (20)$$

3.4. The temperature time derivative

Different methods can be implemented to estimate the time derivative of the temperature needed in the thermal balance equation (1). Due to the noise in the temperature measurements presented paragraph 3.a, we could sample, filter or perform a linear regression on our experimental data. We chose to use OLS linear regression on fitted regression windows. The slope of the fitting line is the derivative of the temperature and is approximated by applying equation (21).

$$\frac{\partial \theta}{\partial t} = \bar{\theta}_t - \bar{\theta}_I \\ \bar{t}^2 - \bar{t}^2 = \frac{\text{Cov}(\theta, t)}{\text{Var}(t)} \quad (^\circ\text{C} \cdot \text{s}^{-1}) \quad (21)$$

These regression windows represent the length of time during which temperatures are being used to calculate the derivative. The thinner the windows, the better the calculated slope matches the temperature derivative from a mathematical point of view. Nevertheless, our measurements are noisy and very thin regression windows lead to unphysical results, so a compromise has to be found. To assign a time to the calculated derivative, we choose the median of the window. However, since the decay heat evolves with time, we decided to adapt the window to the rate at which the temperature changes during the experiment, in order to maintain the best possible balance between noisy and accurate results. Such an adjustment of the time window size had not been performed in the previous analysis of the experiment.

At the early time, narrow regression windows are necessary, otherwise the derivative result will not be representative of the time to which it corresponds, as shown in Fig. 10. The figure shows the temperature time derivative calculated with three different regression windows: 10 min, 20 min and 100 min. The first decay heat value with a 100 min window is obtained 120 min after the scram, as the first data consistent with the isothermal assumption was considered to be obtained at 70 min. The 20 min window also uses temperatures after 70 min, while the 10 min window uses data after 75 min to obtain a first value at 80 min. Looking at Fig. 11, temperatures appear to converge around 70 min, but do not yet represent an isothermal reactor. Two temperatures representing the steam generator outlet are still too different from other temperature measurements. It can be seen that the first value obtained with a 10 min window is 1.5 times higher than with a 20 min window and up to 2 times higher than with a 100 min window. This highlights the problem with the 100 min windows used in the 2012 analysis and the need for a shorter regression window for early times. It also pinpoints the limitations of a point model to represent the reactor. At later times the differences are smaller and come from the noise. With this in mind, we have chosen to reduce the number of decay heat points and reduce the noise effect, thanks to wider regression windows. This makes it easier to compare the measurements with the calculations.

In practice, we have chosen to use a 10 min regression window when the derivative is above 3 °C per hour, a 20 min regression window when it is between 3 and 1 °C per hour and 100 min if it is below 1 °C per hour. We chose these values on the basis of the observations we made in Fig. 10. Before 3 °C per hour, few values are calculated and the noise seems to be negligible compared to the speed at which the derivative evolves. Between 3 °C per hour and 1 °C per hour, we still want to be

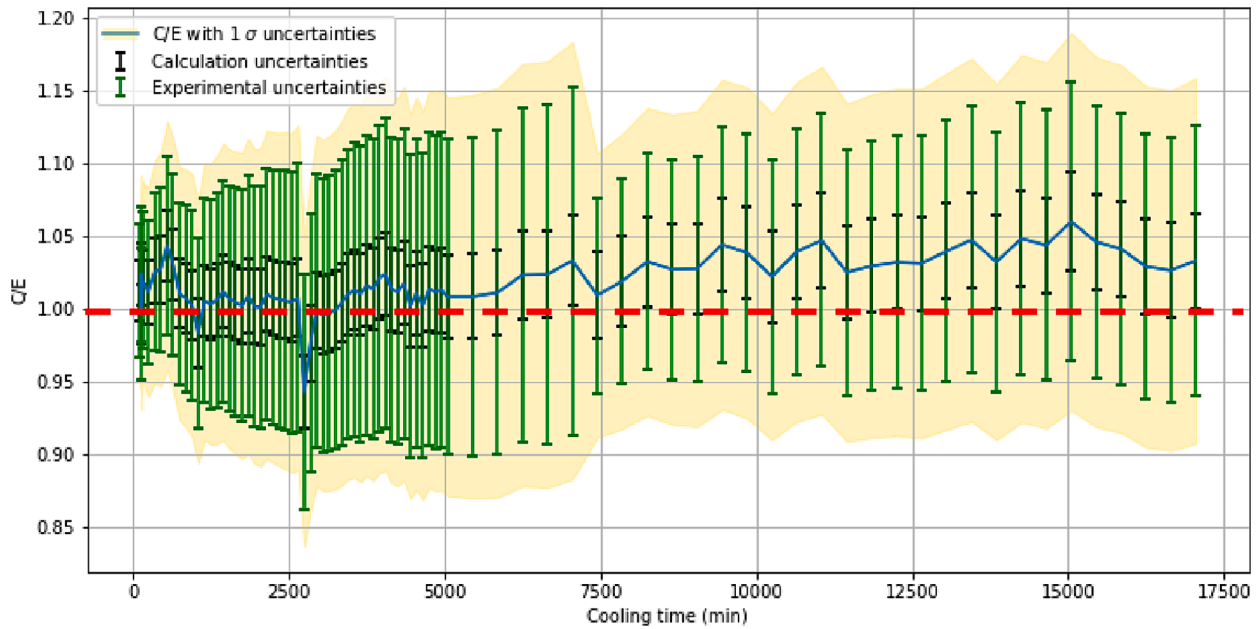


Fig. 15. Discrepancy between the 2016 decay heat calculation and our 2023 measurement re-analysis, with both experimental and calculation uncertainties at 1σ .

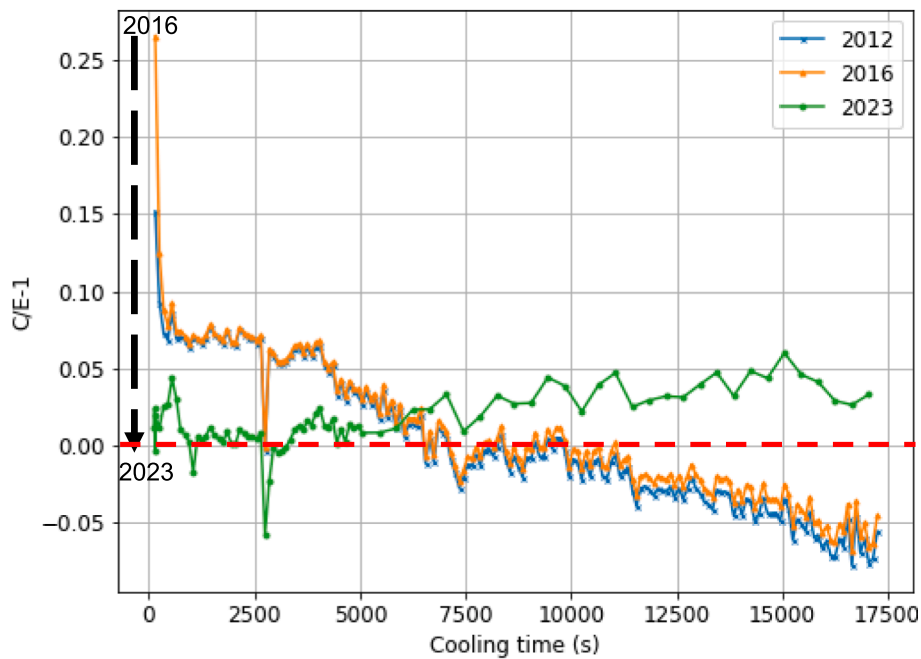


Fig. 16. C/E-1 results on the decay heat for the 2012, 2016 and 2023 studies.

precise enough to avoid erasing possible transients, but the noise starts to be high.

3.5. Experimental uncertainties

We have used the experimental uncertainties given at 1σ by the previous interpretation (Benoit, et al., 2012), which seem to be based on expert advice from the experimental team and are poorly documented:

- a 0.5 % uncertainty for the time derivative of the temperature
- a 5 % uncertainty for inertia, primary pumps and secondary pumps from expert advice

- a 10 % uncertainty for primary and secondary heat leakages from expert advice

3.6. The calculation of the decay heat

The calculation of the decay heat has been described in detail in previous papers (Benoit, 2012) and (Lebrat et al., 2018). The calculation package that was used is DARWIN-2 (Tsilanizara et al., 2000) and the associated nuclear data is the JEFF 3.1.1 library (NEA, 2009). The decay heat calculations are based on the calculation of the isotopic compositions of all reactor subassemblies just prior to the scram. To calculate these compositions, the neutron fluxes are estimated for each reactor cycle in order to perform a depletion calculation based on the neutron

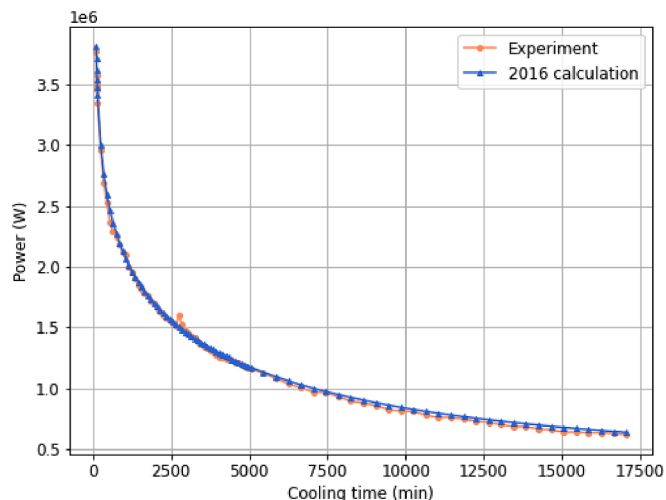


Fig. 17. Comparison between the 2016 decay heat calculation and the 2023 re-analysis of the experiment.

fluxes and previous compositions. This procedure is repeated until the last cycle before the experiment. Given the isotopic compositions at the time the scram is triggered, a final depletion calculation allows us to know the isotopes present in the reactor at each cooling time. Knowing their decay properties, we know how much energy is released thanks to equation (22).

$$P(t) = \sum_i N_i(t) \lambda_i E_i \quad (22)$$

4. Results of our re-analysis of the experiment

We found out that the short times discrepancies between experiment and calculation in the previous decay heat estimate were mainly due to a shift in the time reference during the data processing. The starting point of the experiment was set to 80 min after the scram in the code processing the temperature results. Before this time, the temperatures are not completely homogeneous as shown in Fig. 11 and the fundamental assumption of a thermal “point model” representing the reactor cannot be realistic. In the 2012 decay heat estimate, a 100 min regression window was used and the first experimental value was considered to correspond to 70 min after the scram, but it is in fact 150 min due to the reference time defined by the experimental team. This value had previously been compared with the result of the DARWIN-2 package, which used the time of the scram as the reference time; thus 80 min separated the experimentally estimated values from those calculated.

The effect of the time shift on the C/E discrepancy is important at short times and tends towards zero due to the inverse exponential shape of the decay heat decrease, as shown in Fig. 12. This figure displays the effect of the time shift on the decay heat. It can be observed that between 0 and 2000 min of cooling, the discrepancy is about 10^5 W, while between 15 000 and 17 000 min it is around 10^3 W.

Another source of C/E discrepancy is the calculation of the time derivative of temperature. Calculated by linear regression, it depends on the size of the regression window. At short times, the temperature evolves quickly due to the exponential behaviour of decay heat. To be accurate, a smaller regression window is required as shown in Fig. 10 and explained in paragraph 3.d. This is not the case at longer times, so the width of the window is adjusted to allow a better estimate of the experimental decay heat. We obtain value at earlier times than with only 100 min regression windows, as less data and therefore less experimental time is required to provide a value. These adjusted windows also provide better agreement for early times, as the temperatures used to calculate the rate of temperature change are more representative.

The systematic bias appearing after the emptying of the S3 secondary circuit disappears when using the BILTHER modelling of the primary circuit thermal leakages, as shown in Fig. 13. For both models, we have implemented the same regression windows for the calculation of temperature rate of change and no time shift was present. At about 5 000 min, we can observe an intersection between the curves based on the ETNa and BILTHER thermal modelling. Fig. 14 highlights even more the bias represented by the fall of the ETNa C/E after 5 000 min. The BILTHER model shows better C/E at short and very long times. There might be another possible subtle bias estimated at about 15 kW. However, given the uncertainties shown in Fig. 15, it does not seem relevant to investigate further.

This explains why the subsequent decay heat calculations still showed large discrepancies with the previous experimental results: the decay heat “measurements” are obtained through data interpretation and post-processing, which make them difficult to obtain. The reactor has undergone many changes during its operation, including a change of power. Since the 1990’s, the thermal power of the reactor has been reduced from 530 to 350 MWt, resulting in a configuration with two secondary loops instead of three. However, the ETNa models used data prior to the reconfiguration, implying a possible bias. It is very likely that the thermal behaviour of the reactor changed over time and partly because of the S2 secondary circuit emptying, which probably changed the temperature distribution in the reactor. The BILTHER model was designed after the power change and validated with data from operation with two secondary loops. Replacement of materials and ageing of components might also have changed the thermal behaviour of the reactor components, since almost 40 years separate the first model used in the previous estimate and the PUIREX experiment.

With our re-analysis of the experimental data, we observe in Fig. 16 that the C/E discrepancy on the decay heat is now between + 6 % and – 1 % instead of a + 26 % to – 6 % previously. A few points are below – 1 % and have a known source: they are due to human intervention on the reactor operating conditions, for which the thermal modelling is not accurate enough to calculate the decay heat accurately during such transients. Nevertheless, experimental uncertainties are too large to warrant a search for a better model at this stage.

5. Conclusion

Our estimate of the decay heat during the PUIREX experiment now shows a very good consistency with the latest 2016 calculation, as shown in Fig. 17. Compared to the previous 2012 estimate, some improvements have been made in the time reference, the temperature variation rate and the model of the primary thermal leaks. The new – and smaller – discrepancies between the experimental results and the calculation are great news for the understanding of the experiment and the validation of the DARWIN-2 depletion package. It highlights the significance of the data processing and comforts the validity of models used during the Phénix operation and the validity of the codes. It also raises questions about the discrepancies between the other experiments and the corresponding calculations mentioned in Table 1. Similar investigations will be carried out to see if they can also be explained by the way the data processing was performed.

Declaration of competing interest

The authors declare that they have no known competing financial interests or personal relationships that could have appeared to influence the work reported in this paper.

Data availability

The authors do not have permission to share data.

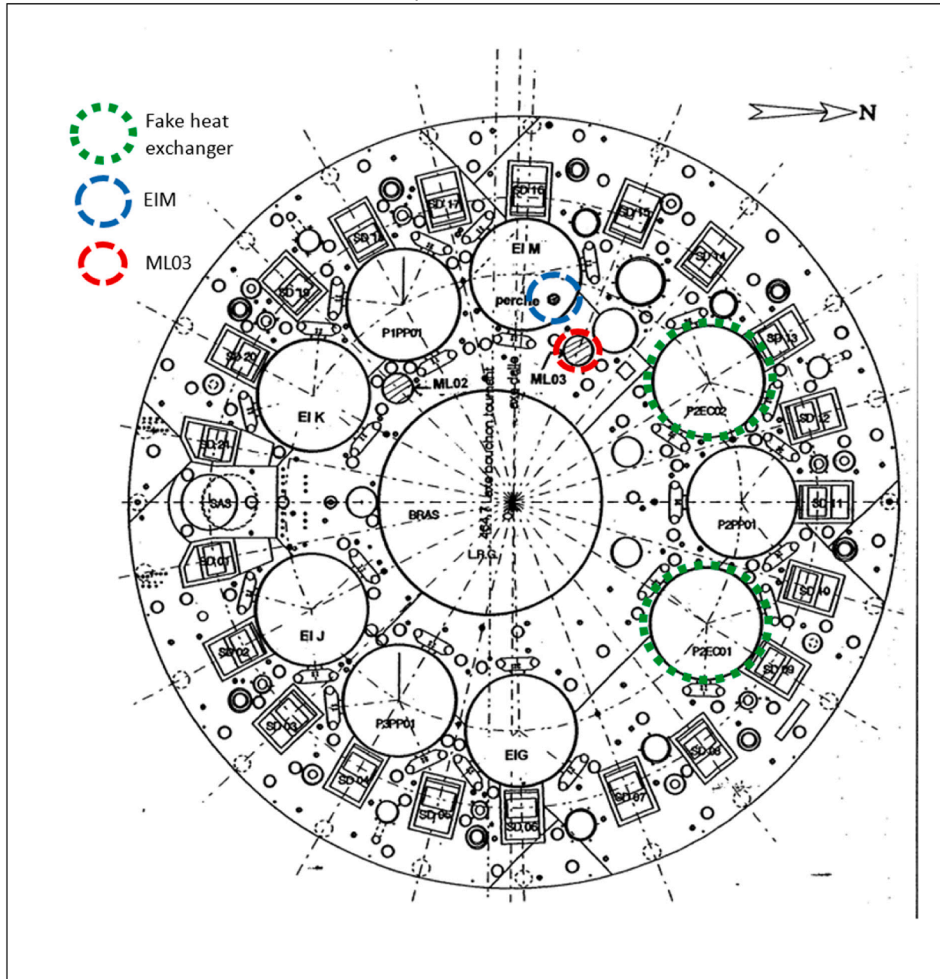
Acknowledgments

The authors acknowledge EDF for its financial support.

Appendices

A. Location of the thermocouples used.

A. Location of the thermocouples used



Appendix 1. . Location of fake exchangers and the two-instrumented poles, which gathered temperatures during the 2008 PUIREX experiment.

References

- Akiyama, M., et al., 1982. Measurements of Gamma-Ray Decay Heat of Fission Products or Fast Neutron Fissions of ^{235}U , ^{239}Pu and ^{233}U . *J. Nucl. Sci. Technol.* 24, 9.
- Algora, A., et al., 2010. Reactor decay heat in ^{239}Pu : solving the γ discrepancy in the 4-3000-s cooling period. *Phys. Rev. Lett.* 150 <https://doi.org/10.1103/PhysRevLett.105.202501>.
- Aoyama, T., et al., 1999. Measurement and analysis of decay heat of fast reactor spent fuel. In: *JAERI-Conf 99-002*, pp. 84-91.
- Appere, "Présentation du code de calcul ETNA - Description des modèles", private communication, (1998).
- Auban, O., "Compte rendu d'essai "PUIREX", Mesure expérimentale de la puissance résiduelle du réacteur PHENIX durant l'arrêt programmé A9", private communication, (2008).
- Bell, 1973. "ORIGEN B-The ORNL Isotope Generation and Depletion Code", Technical Report ORNL-4628 (CCC-217), Union Carbide Corporation (Nuclear Division). Oak Ridge National Laboratory.
- Benoit, J.C., 2012. Développement d'un code de propagation des incertitudes des données nucléaires sur la puissance résiduelle dans les réacteurs à neutrons rapides". *Physique Nucléaire Théorique Université Paris Sud - Paris XI*.
- Benoit, J.C., et al., Decay Heat of Sodium Fast Reactor: Comparison of Experimental Measurements on the PHENIX reactor with Calculations performed with the French DARWIN package, *PHYSOR 2012*, Knoxville, Tennessee, USA, April 15-20, (2012), https://inis.iaea.org/search/search.aspx?orig_q=RN:44063643.
- Bernardin, B., "Interprétation de la mesure de puissance résiduelle à SPX, Essai du 25 Novembre 1996", private communication, (1998).
- Bourdot, P., "Qualification du formulaire DARWIN-RNR pour le calcul de la puissance résiduelle. Interprétation du 22/11/96 à SUPERPHENIX", private communication, (2002).
- Calame, A., et al., "Analysis of a decay heat experiment in SUPERPHENIX for the experimental validation of the DARWIN3 package", BEPU, Giardini Naxos, Sicily, Italy, October 11-17, (2020).
- Chauchepat, P., et al., Experimental measurement of the decay power in the phenix fast reactor", *NUTHOS-7*, Seoul, Korea, October 5-9, (2008).
- Coulon, R., 2010. *Spectrométrie gamma haute résolution et hauts taux de comptage sur primaire de réacteur de type génération 4 au sodium liquide.* (physics.ins-det). université De Caen.
- Desperts, "Essai No. 572: Mesure de la puissance résiduelle, compte rendu de l'essai", private communication, (1979).
- Dickens, J.K., et al., 1977. Fission-Product Energy Release for Times following Thermal-Neutron fission of ^{235}U Between 2 and 14 000 s. Technical Report ORNL NUREG-14.

- Dickens, J.K., et al., "Fission-Product Energy Release for Times Following Thermal-Neutron Fission of ^{239}Pu and $^{241}\text{Plutonium}$ Between 2 and 14 000 s", Nucl. Sci. Eng., Vol. 78, No. 126, (1981).
- Duchemin, B., et al., "Decay heat calculation : An International Nuclear Code Comparison", NEACRP-139-L, NEANDC-275-U, (1990).
- Dumarcher, V., et al., "Assessment and Management of Sodium Temperature during Phénix Reactor Maintenance Stops", NUTHOS-7, Seoul, Korea, October 5-9, (2008).
- England, T.R., "Cinder – A One-point Depletion and Fission Product Program", WAPD-TM-334, Bettis Atomic Power Laboratory, Pittsburgh, Pennsylvania, (1962).
- Fisher, P.C., et al., "Decayed Gammas from Fast-Neutron Fission of Th^{232} , U^{233} , U^{235} , U^{238} and Pu^{239} ", Phys. Rev., Vol. 134 No. 4B, (1964). <https://doi.org/10.1103/PhysRev.134.B796>.
- Foust, O. J., 1972. *Sodium-NaK engineering handbook* / O.J. Foust, editor Gordon and Breach New York.
- Gillet, G., "Mesure de la puissance résiduelle à SPX1", technical document, *private communication*, (1987).
- Gillet, G., "Puissance résiduelle de SPX1, mesure et comparaison calcul-experience", *private communication*, (1988).
- Gillet, G., "Réacteur Phénix: Interprétation de la mesure de la puissance résiduelle avec le formulaire de calcul", *private communication*, (1992).
- Gillet, G., "Interprétation de la mesure de puissance résiduelle Phénix - 22 février 1993-essai 841", *private communication*, (1993).
- Gillet, G., "Interprétation de la mesure de puissance résiduelle effectuée à SUPER-PHENIX le 26 Mai 1987 en utilisant les données de base issues de JEFF.1", *private communication*, (1996).
- Gillet, G., et al., 1990. Measurement of Decay Heat and Comparison with Predictions. Nucl. Sci. Eng. 106, 94–97. <https://doi.org/10.13182/NSE90-A23763>.
- Gomin, et al., 1999. The MCU Monte Carlo Code for 3D Depletion Calculation. Proceedings of International Conference, 2, Madrid, Spain.
- Grouiller, J.P., et al., 1990. Cycle du combustible des réacteurs à neutrons rapides—système de codes MECCYCO. Proceedings of the Int. Conf. on the Physics of Reactors: Operation, Design and Computation.
- Guadilla, V., et al., 2016. First experiment with the NUSTAR/FAIR decay total absorption γ -ray spectrometer (DTAS) at the IGISOL IV facility. Nucl. Instrum. Methods Phys. Res. B 376, 334–337. <https://doi.org/10.1016/j.nimb.2015.12.018>.
- Guidez, J., 2013. Phénix: The Experience Feedback. EDP Sciences, Paris.
- Guidez, J., "Compte-rendu de l'essai n° 644 : Mesure de la puissance résiduelle", *private communication*, (1983).
- Hardy, J.C., et al., 1977. The essential decay of Pandemonium: a demonstration of errors in complex Beta-Decay schemes. Phys. Lett 71 B (2). [https://doi.org/10.1016/0375-9474\(78\)90162-8](https://doi.org/10.1016/0375-9474(78)90162-8).
- Ilas, G., et al., 2008. SCALE analysis of CLAB decay heat measurements for LWR spent fuel assemblies. Ann. Nucl. Eng. 35, 37–48. <https://doi.org/10.1016/j.anucene.2007.05.017>.
- Jaboulay, J.C., et al., Analysis of MERCI Decay Heat Measurement for PWR UO_2 Fuel Rod, Nuclear Technology, 177:1, pp. 73-82, (2012). <https://doi.org/10.13182/NT12-A13328>.
- Jockey, 1963. The advantage of using the Henry straight line in γ spectrometry. CEA Rep. 2296. <https://www.osti.gov/etdweb/servlets/purl/20808550>.
- Johnston, K., 1964, A calorimetric determination of fission product heating in fast reactor plutonium fuel, Journal of Nuclear Energy Parts A/B, 1965, Vol. 19, pp. 527-539.
- Kolobashkin, V.M., et al., 1983. Radiation Characteristics of Irradiated Nuclear Fuel. Energoatomizdat Publications, Moscow, p. 51.
- Lebrat, J.F., et al., 2018. Uncertainty assessment on the calculated decay heat of the ASTRID basic design core based on the DARWIN-2.3 package. Ann. Nucl. Eng. 120, 378–391. <https://doi.org/10.1016/j.anucene.2018.05.043>.
- Lebrat, J.F., et al., "Interprétation de l'essai de puissance résiduelle PUIREX 2008 avec le formulaire DARWIN-2.3 associée au code d'incertitudes CYRUS", *private communication*, (2016).
- Lott, M., et al., 1972. Puissance résiduelle totale émise par les produits de fission thermique de ^{235}U . J. Nucl. Energy. 27, 597–605. [https://doi.org/10.1016/0022-3107\(73\)90020-8](https://doi.org/10.1016/0022-3107(73)90020-8).
- Maekawa, F., et al., 2000. Development of whole energy absorption spectrometer for decay heat measurement. Nucl. Instrum. Methods Phys. Res. A 450, 467–478. [https://doi.org/10.1016/S0168-9002\(00\)00301-6](https://doi.org/10.1016/S0168-9002(00)00301-6).
- Martin, L., "Mesure de la puissance résiduelle après 10 jours de fonctionnement à 350 MW", *private communication*, (1993).
- The JEFF-3.1.1 Nuclear Data Library "JEFF Report 22", 2009, http://www.oecd-nea.org/dbdata/nds_jefreports/jefreport-22/nea6807-jeff22.pdf.
- Nguyen, H., "Decay heat measurements following neutron fission of ^{235}U and ^{239}Pu ", International Conference on Nuclear Data for Science and Technology, Trieste, Italy, (1997).
- Schrock, V.E., 1979. Evaluation of decay heating in shutdown reactors. Prog. Nucl. Energy 3, 125–126. [https://doi.org/10.1016/0149-1970\(79\)90013-1](https://doi.org/10.1016/0149-1970(79)90013-1).
- Shure, K., "Fission-Product Decay Energy", In USAEC Report WAPD-BT-24, pp. 1-17, (1961).
- Svensk Kärnbränslehantering, A.B., 2006. Measurements of decay heat in spent nuclear fuel at the Swedish interim storage facility. Clab, Swedish Nuclear Fuel and Waste Management report R-05-62.
- Tasaka, K., 1977. DCHAIN: Code for Analysis of Build-up and Decay of Nuclides. JAERI report No.1250.
- Tsilanizara, A., et al., 2000. DARWIN: An evolution code system for a large range of applications. J. Nucl. Sci. Technol. Supplement 1, 845–849. <https://doi.org/10.1080/00223131.2000.10875009>.
- Wilk, M.B., et al., 1968. Probability plotting methods for the analysis of data, Biometrika Vol. 55, 1, pp. 1-17. <https://doi.org/10.1093/biomet/55.1.1>.